Journal of Advanced Ceramics
2014, 3(2): 98–108
DOI: 10.1007/s40145-014-0098-9

ISSN 2226-4108
CN 10-1154/TQ

Research Article

Effect of Li^+ ion mobility on the grain boundary conductivity of Li_2TiO_3 nanoceramics

Umasankar DASH[a,*], Subhanarayan SAHOO[b], S. K. S. PARASHAR[a], Paritosh CHAUDHURI[c]

[a]*School of Applied Sciences*, *KIIT University Bhubaneswar-751 024*, *India*
[b]*Department of Electrical and Electronics Engineering*, *Trident Academy of Technology*, *Bhubaneswar-751 024*, *India*
[c]*Institute for Plasma Research*, *Bhat*, *Gandhinagar*, *Gujurat-382 428*, *India*

Received: September 08, 2013; Revised: February 06, 2014; Accepted: February 19, 2014

Abstract: Lithium titanate (Li_2TiO_3) is one of the most promising candidates among the tritium breeding materials because of its good tritium release capacity. Li concentration has much significance on the diffusivity of tritium in the material. The nanocrystalline single-phase Li_2TiO_3 with monoclinic structure has been prepared by high energy ball milling followed by calcination at 700 ℃ for 2 h. The field emission scanning electron microscopy (FESEM) studies confirmed uniform distribution of nanocrystalline phase with particle size below 100 nm. The study of the Li^+ ion diffusion on the sintered sample was investigated by means of electrical conductivity measurements. Electrical properties of the samples were studied in wide temperature (50–500 ℃) and frequency (100 Hz–1 MHz) ranges. The complex impedance spectroscopy (CIS) studies showed the presence of both bulk and grain boundary effects in nanocrystalline Li_2TiO_3. The bulk resistance of the samples has been observed to decrease with rise in temperature showing a typical negative temperature coefficient of resistance (NTCR) behavior. The low activation energies of the samples suggested the presence of singly ionized oxygen vacancies in the conduction process. The hopping frequency shifted toward higher frequency with increase in temperature. Activation energy of 0.86 eV was calculated from AC conductivity.

Keywords: high energy ball milling; AC conductivity; impedance spectroscopy; nanocrystalline

1 Introduction

Lithium titanate (Li_2TiO_3) has attracted many researchers due to its distinguished properties as one of the most promising solid breeding materials in the blanket of future nuclear fusion reactor. It shows good chemical stability in air [1] and acceptable mechanical strength [2], and displays compatibility with other structural components [3], adequate irradiation behavior [4], and low activation and excellent tritium release characteristics at lower temperatures [5,6]. This tritium breeder is most commonly used as pebble or pellet. Significant work has been done on the fabrication of Li_2TiO_3 pebbles [7–16]. Tritium release is one of the most important features for breeding materials [17].

In the D–T fusion reactor, the energy conversion from ^6Li to tritium occurs in various steps as

$$D + T \rightarrow (He + 3.52\ MeV) + (n + 14.1\ MeV) \quad (1)$$

* Corresponding author.
E-mail: dashumasankar@gmail.com

The role of ^{6}Li is to produce tritium via interaction with neutron:

$$^6\mathrm{Li} + \mathrm{n} \rightarrow (\mathrm{He} + 3.52\ \mathrm{MeV}) + (\mathrm{n} + 14.1\ \mathrm{MeV}) \quad (2)$$

A variety of chemical methods, such as solid state reaction process, sol–gel [18], wet chemical method [19], solution combustion [20] and extrusion–spheronisation–sintering method [21,22], have been tried for the synthesis of Li_2TiO_3, and these techniques allow the preparation of stoichiometric single-phase material after high-temperature calcination. In the present study, nanocrystalline Li_2TiO_3 has been synthesized by high energy ball milling followed by calcinations at 700 ℃. Complex impedance spectroscopy (CIS) technique has been applied to analyze the electrical behavior of nanocrystalline Li_2TiO_3. Literature survey reveals that less work has been carried out so far in understanding the electrical properties of Li_2TiO_3 nanoceramic. Therefore, we have made an attempt to carry out a detailed study on the electrical properties of nanocrystalline Li_2TiO_3 using CIS.

2 Mechanism

In this article, there is an extensive use of mechanical alloying for the formation of single-phase nanocrystalline material. Mechanical alloying (MA) refers to milling process of homogenous compositions where mass transfer is not required. Therefore, it is often associated with milling of pure metal oxides which are in thermodynamic equilibrium with each other. In mechanical alloying, there involves chemical reaction, nucleation, structural change, and growth of nanocrystalline material which in turn gives compounds that need no further calcination or annealing. It is commonly believed that in mechanical alloying, mechanical activation can significantly increase the grain refinement, crystal structure, and reactivity of solid system with various structural and surface defects. This enhances the reaction kinematics to be played into account. This is supported by much lower calcination and phase formation temperatures. In order for a particle to aggregate and fragment, it must be involved in a collision between milling media. Particles will experience collisions at different frequencies depending on their sizes, and variation must be reflected in both aggregation and fragmentation rates. In studying the mechanism, it finds the importance of co-ordinate states, symmetry disturbance and change in electronic states. One of the common processes that occur in the case of mechanical milling is the evolution of stress and some shear components which creates crystal deformation and change in lattice parameters.

3 Complex impedance spectroscopy

Complex impedance spectroscopy (CIS) is a very powerful technique for characterization of electrical behavior of materials. CIS describes the electrical phenomena occuring in the material by applying AC perturbation signal. The output response plotted in a complex plane represents succession of semicircles due to bulk properties, grain boundary and electrode process in the system. In CIS, the grain and grain boundary contributions are represented by semicircles; wherein the grain contribution represents the bulk properties of the material, whereas the grain boundary contribution arises from the partial or complete blocking of charge carriers at low frequencies. The contribution due to bulk properties of the material is noticeable only at high-frequency domain. The bulk properties of all individual grains contribute directly to give the overall effective bulk resistance (R_b) and geometrical capacitance of the domain (C_b).

The data can be analyzed in four different ways, i.e., impedance (Z^*), admittance (Y^*), permittivity (ε^*) and electrical modulus (M^*) [23]. They are related to others as follows:

$$M^* = \mathrm{j}\omega\varepsilon_0 Z^* \quad (3)$$

$$Z^* = R_s - 1/(\mathrm{j}\varepsilon C_s) \quad (4)$$

$$Y^* = \mathrm{j}\omega\varepsilon_0\varepsilon^* \quad (5)$$

$$\varepsilon^* = 1/M^* \quad (6)$$

where ω is the angular frequency, $\omega = 2\pi f$; ε_0 is the permittivity of free space; R_s and C_s are the resistance and capacitance in series, respectively. In order to explain the experimental data, it is essential to design an equivalent circuit and fit the circuit to the obtained data which will provide the realistic representation of electrical properties. This can be best understood by combining impedance and modulus formalisms.

4 Experiment

Nanocrystalline Li_2TiO_3 powder was synthesized by

mechanochemical route. The precursors (Li_2CO_3 and TiO_2) were taken in a stoichiometric ratio. The mixture was milled using a high energy planetary ball mill (PM 400) under atmospheric conditions using tungsten carbide balls. The milling was continued for 30 min to avoid an excess temperature increase inside the milling jar. The milled powder was calcined at 700 ℃ for 2 h. The synthesized powder was characterized with respect to phase identification and lattice parameter measurements, using X-ray diffraction (XRD) with Cu Kα (PANalytical, X'pert Pro). It has been observed that single-phase monoclinic structure was obtained at 700 ℃. The calcined powder was pressed uniaxially at 200 MPa with 3 wt% PVA solution added as binder. The green pellets were sintered at 700 ℃ for 2 h. The microstructure and average grain size were studied by field emission gun scanning electron microscope (FEGSEM-ZEISS). Silver contacts were made on the opposite disc faces and heated at 700 ℃ for 15 min for electrical measurement. The CIS and conductivity measurement were carried out in a frequency range of 100 Hz to 1 MHz using LCR meter HiTESTER 3532-50 (Hioki, Japan). The process is shown in Scheme 1.

5 Results and discussion

5.1 Structure and microstructure of fractured surfaces

Figure 1 shows the XRD pattern of the Li_2TiO_3 powder calcinied at 700 ℃ for 2 h. It is observed that single-phase monoclinic structure with space group *C*2/*c* (JCPDS No. 33-0831) and lattice parameters of a = 5.069 Å, b = 8.799 Å and c = 9.759 Å was formed at 700 ℃. The average crystallite size of the powder is 30 nm, as determined from X-ray peak broadening using a Voigt peak profile analysis after eliminating the instrumental broadening and strain contributions. The FESEM micrograph in Fig. 2 shows that nanocrystalline Li_2TiO_3 sintered at 700 ℃ has uniform grain size.

5.2 CIS study

CIS study shows two successive semicircles comprising bulk (R_b) and grain boundary (R_{gb}) resistance. R_b and R_{gb} are calculated and the values are shown in Table 1. The bulk electrical conductivity (σ_b) can be written as

$$\sigma_b = \frac{1}{R_b} \times \frac{l}{A} \tag{7}$$

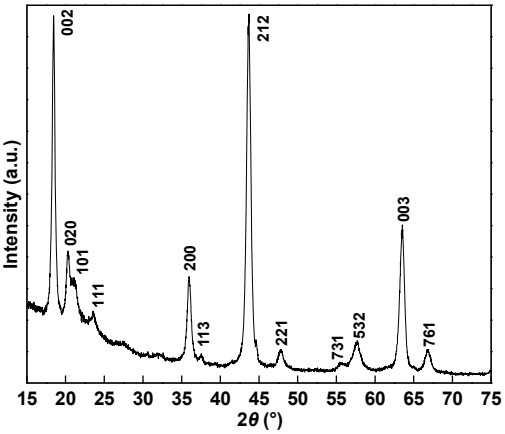

Fig. 1 XRD pattern of nanocrystalline Li_2TiO_3.

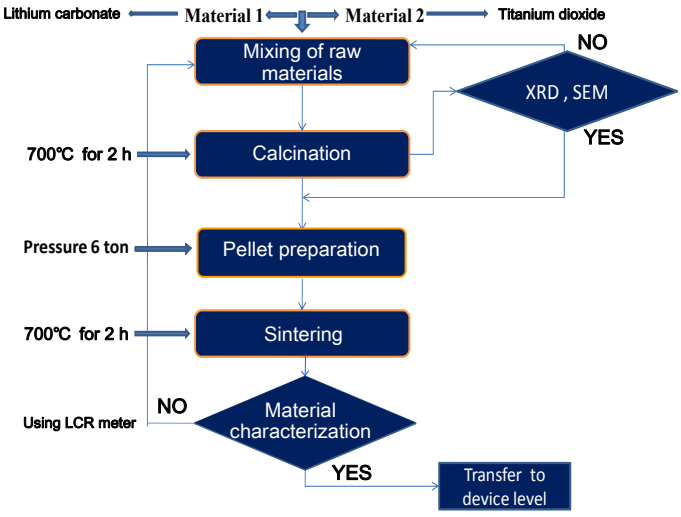

Scheme 1 Process of material synthesis.

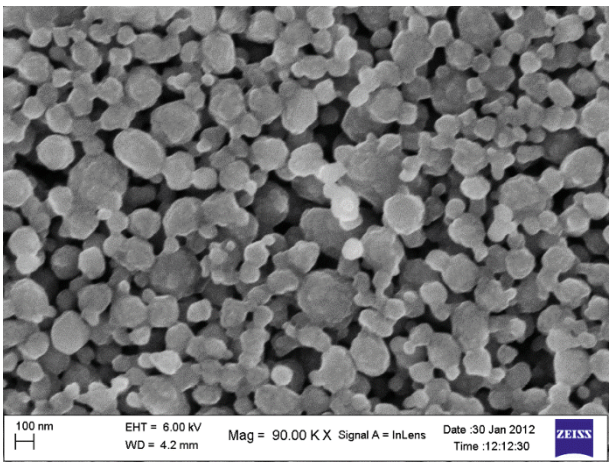

Fig. 2 FESEM micrograph of nanocrystalline Li_2TiO_3.

Table 1 Bulk resistance (R_b), bulk capacitance (C_b), relaxation frequency (f_0) and grain boundary resistance (R_{gb}) of Li_2TiO_3 nanoceramic samples and (ωR_bC_b) as product

Sample	T (℃)	R_b (Ω)	C_b (F)	f_0 (Hz)	R_{gb} (Ω)	ωR_bC_b
1	200	1.05×10^6	1.01069×10^{-9}	1.5×10^2	3.3×10^6	0.9999
2	225	6.50×10^5	6.12249×10^{-10}	4.0×10^2	11.5×10^5	0.9999
3	250	4.80×10^5	1.65817×10^{-10}	2.0×10^3	5.1×10^5	0.9999
4	275	3.40×10^5	7.80318×10^{-11}	6.0×10^3	2.6×10^5	0.9999
5	300	2.40×10^5	4.42180×10^{-11}	15×10^3	1.1×10^5	0.9999
6	325	1.68×10^5	3.79011×10^{-11}	25×10^3	5.4×10^4	0.9999
7	350	1.02×10^5	3.45116×10^{-11}	45×10^3	4.0×10^4	0.9999
8	375	6.80×10^4	3.90159×10^{-11}	6.0×10^4	3.2×10^4	0.9999
9	400	4.50×10^4	3.93049×10^{-11}	9.0×10^4	1.75×10^4	0.9999
10	425	2.80×10^4	2.84258×10^{-11}	2.0×10^5	1.0×10^4	0.9999
11	450	1.75×10^4	2.59893×10^{-11}	3.5×10^5	5.5×10^3	0.9999
12	475	1.18×10^4	2.24837×10^{-11}	6.0×10^5	4.0×10^3	0.9999
13	500	7.80×10^3	2.72111×10^{-11}	7.5×10^5	2.8×10^3	0.9999

where l is the thickness and A is the area of the electrode deposited on the sample. The relaxation frequency (f_0) is calculated from the maximum value of the imaginary parts of the CIS plot (f vs. Z'') [24]. This can be related as

$$2\pi f_0 R_b C_b = 1 \tag{8}$$

where C_b is the bulk capacitance. The value of C_b can be calculated from

$$C_b = \frac{1}{2\pi f_0 R_b} \tag{9}$$

Figure 3 shows the variation of real part of impedance Z' with frequency at different temperatures. The magnitude of Z' decreases with increasing temperature, which indicates an increase in AC conductivity. It is also observed that the magnitude of Z' decreases with increasing temperature as well as frequency, indicating negative temperature coefficient of resistance (NTCR) behavior of Li_2TiO_3. At higher frequencies, the values of Z' are almost equal for all the temperatures, which clearly indicates the presence of space charge polarization. The higher impedance value at lower frequencies also indicates the presence of space charge polarization in the material [25]. Figure 4 shows the variation of Z'' with frequency at different temperatures. It is found that Z'' values attain a peak (Z''_{max}) at a certain frequency at all the measured temperatures, which shifts to higher frequency with increasing temperature. Figure 4 also shows that the peak Z''_{max} shifts to higher frequency with increase in temperature, and all

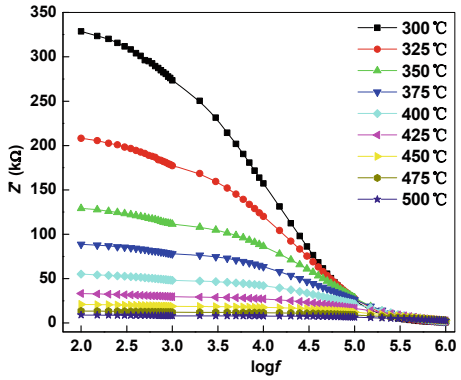

Fig. 3 Variation of real part of complex impedance Z' with log$f$ at different temperatures.

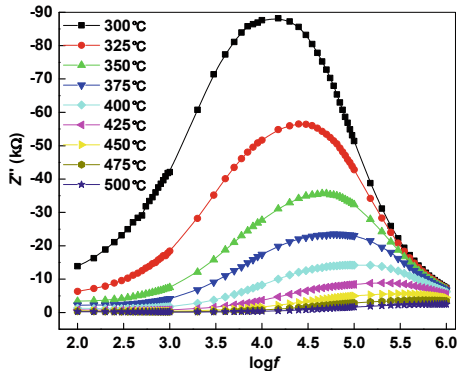

Fig. 4 Variation of imaginary part of complex impedance Z'' with log$f$ at different temperatures.

the curves merge at higher frequencies. The shifting of peaks towards higher frequency indicates that the relaxation time decreases with the increase of temperature. The peak broadening with increasing

temperature suggests the presence of temperature-dependent electrical relaxation phenomenon in the material. The asymmetric broadening of peaks in frequency explicit plots of Z'' is observed in Fig. 4. It confirms the spread of relaxation time [26], i.e., the existence of a temperature-dependent electrical relaxation phenomenon in nanocrystalline Li_2TiO_3. The relaxation process is due to the presence of space charge whose mobility increases at higher temperature.

Figures 5 and 6 show the variation of relaxation time and relaxation frequency with inverse of temperature. The activation energy is found to be 0.86 eV from Fig. 5. The relaxation time (τ) was calculated from the peak position of Z'' versus frequency plot using the relation $2\pi f_0\tau = 1$, where f_0 is the relaxation frequency. The plot of τ versus $1000/T$ gives a straight line, which can be approximated to the relation $\tau = \tau_0 \exp[-E_a/(k_B T)]$, where τ_0 is the pre-exponential factor; E_a is the activation energy; and k_B is the Boltzmann constant.

Figures 7(a) and 7(b) show Cole–Cole formalisms of the Li_2TiO_3 samples at different temperatures. It is observed that at different temperatures two depressed semicircles are observed, which confirms the presence of both grain interior (bulk property) and grain boundary effect. However, with the increase of temperature from 200 ℃ to 500 ℃ the grain boundary contribution (R_{gb}) decreases as shown in Fig. 7 and Table 1. All the semicircles exhibit some depression instead of a semicircle centered on real axis Z' due to a distribution of relaxation time. These depressed semicircles represent a constant phase element (CPE) in the equivalent circuits. In the case of ceramic materials, a distribution of relaxation time is usually observed and the capacitance is replaced by a CPE, which represents more accurately the behavior of the grain interior and grain boundary processes. A CPE is characterized by two parameters. The admittance $Y^*(\omega)$ of CPE can be defined as follows:

$$Y^*(\omega) = A(\mathrm{j}\omega)^P \tag{10}$$

where coefficient A relates to the size, thickness and material properties of a capacitor; and P is the degree of the energy dissipation. The CPE causes depression of the ideal semicircle, observed on the complex plane plots by an angle:

$$\beta = (1-P)\frac{\pi}{2} \tag{11}$$

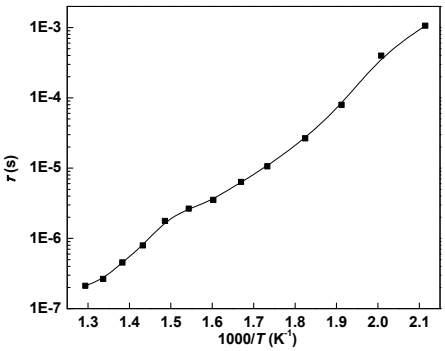

Fig. 5 Variation of relaxation time with inverse of temperature.

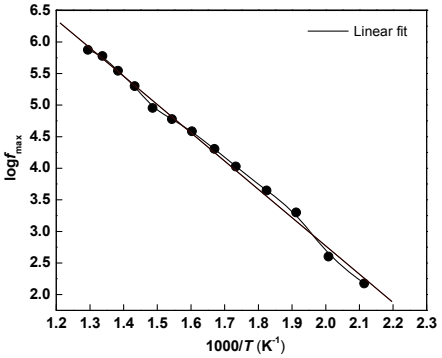

Fig. 6 Temperature dependence of relaxation frequency of Li_2TiO_3 nanoceramics.

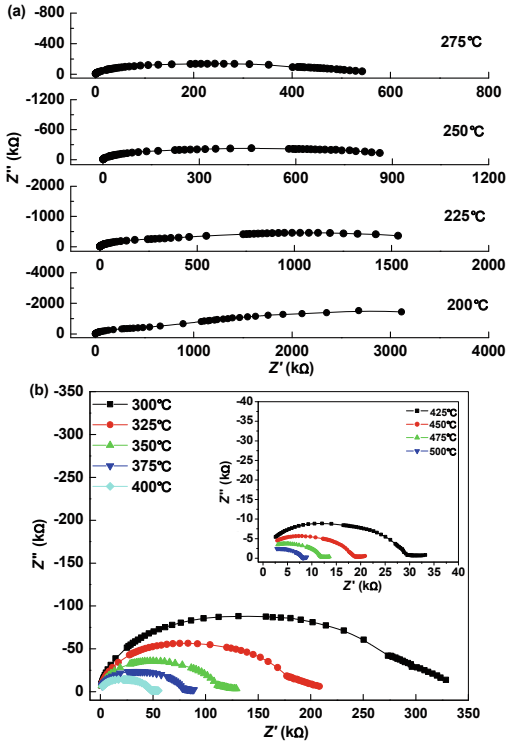

Fig. 7 Variation of real (Z') and imaginary (Z'') parts of complex impedance at different temperatures: (a) from 200 ℃ to 275 ℃; (b) from 300 ℃ to 400 ℃ (inset from 425 ℃ to 500 ℃).

where β is the depression angle. Separation of the bulk and grain boundary of the material is obtained by fitting the experimental response to that of an equivalent circuit, which is usually considered to comprise a series of two parallel resistor elements. The depression of the semicircle is considered to be a further evidence of polarization phenomena with a distribution of relaxation time. This can be referred to as the non-Debye type of relaxation in which there is a distribution of relaxation time. This non-ideal behavior can be correlated to several factors, such as grain orientation, grain boundary, stress–strain phenomena and atomic defect distribution. The contribution positioned at low frequency corresponds to the grain boundary response, and in the high frequency, it corresponds to the specific property of the bulk. As seen from Fig. 7, the total resistance of the sample decreases with increase in temperature.

5.3 Conductivity analysis

The AC conductivity variation with frequency is shown in Fig. 8. It is observed that the slope changes in the AC conductivity spectra at a particular frequency, which is known as the "hopping frequency (ω_p)". The value of AC conductivity can easily be understood from the power law [27] given by

$$\sigma(\omega) = A(T)\omega^n + \sigma(T) \tag{12}$$

where $A(T)$ is a pre-exponential factor dependent on temperature; $\sigma(T)$ corresponds to the DC conductivity; and n is a universal factor. It is a function of both temperature and frequency, and corresponds to short-range hopping of charge carriers through trap sites separated by energy barriers of varied heights. Each pair of potentials corresponds well to a certain time constant of transition from one site to another. The time constant for transition across a higher energy barrier is large compared to smaller ones, and therefore, traps with high activation energy can respond at low frequencies. The dispersion in conductivity at low frequency can be explained due to non-adiabatic hopping of charge carriers between impurity sites. Figures 9 shows the Arrhenius plot of AC conductivity of nanocrystalline Li_2TiO_3 while Figure 10 shows DC conductivity with inverse of temperature. It is found that the plot of $\log\sigma_{DC}$ against $1000/T$ is linear and fits well with the Arrhenius equation:

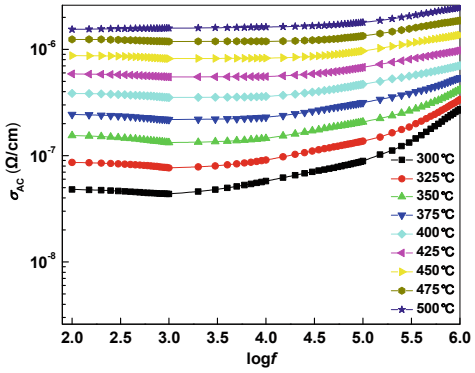

Fig. 8 Variation of AC conductivity with $\log f$ at different temperatures.

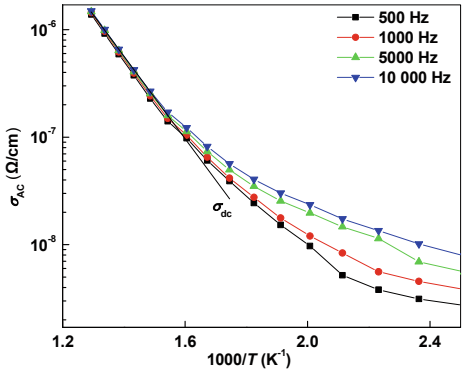

Fig. 9 Arrhenius plot of AC conductivity of Li_2TiO_3 nanoceramics.

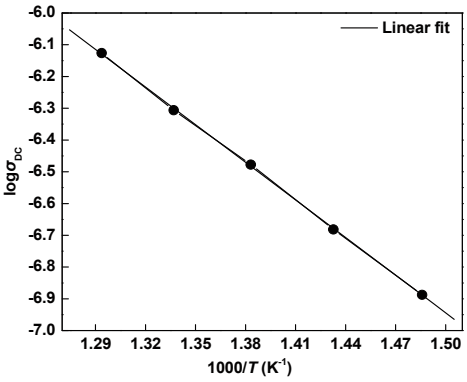

Fig.10 Variation of DC conductivity with inverse of temperature.

$$\sigma_{DC} = A\exp\left(-\frac{E_a}{k_B T}\right) \tag{13}$$

where A is the pre-exponential factor; E_a is the activation energy for conduction; and k_B is the Boltzmann constant. The pre-exponential factor is constant for the same material system and does not vary with the activation energy or the temperatures. The conductivity enhances greatly with the increase of temperature. In ceramic samples, usually oxygen

vacancies are considered as one of the mobile charge carriers. The ionization of oxygen vacancies creates conducting electrons, which are easily thermally activated. It clearly suggests a possibility that the conduction in the higher-temperature range for charge carriers may be oxygen vacancies. The bulk conductivities of Li_2TiO_3 at higher temperature are evaluated from Fig. 7 using the relation:

$$\sigma_{\mathrm{b}} = \frac{1}{R_{\mathrm{b}}} \times \frac{l}{A} \tag{14}$$

where R_{b} is the bulk resistance; l is the thickness; and A is the area of the electrode. The value of bulk resistance R_{b} and grain boundary resistance R_{gb} are obtained from the high-frequency and low-frequency intercepts of the semicircle on the real axis (Z' axis) in the complex impedance plot. The conductivity variation indicates an increase of conductivity with rise in temperature with a typical Arrhenius-type behavior having linear dependence on logarithm of conductivity. The type of temperature dependence of DC conductivity indicates that the electrical conduction in the material is a thermally activated process. The activation energy is calculated from the linear portion of the plot of DC conductivity versus $10^3/T$. It is found that activation energy (0.86 eV) is nearly equivalent to the value calculated from relaxation time.

5.4 Modulus study

Electrical response can be analyzed by complex formalism by plotting real and imaginary parts of modulus with different frequencies. The electrical modulus can be represented as

$$M^*(\omega) = \mathrm{j}\omega C_0 Z^*(\omega) \tag{15}$$

where C_0 is the vacuum capacitance. Electrical modulus can be understood in terms of reciprocal of the permittivity:

$$M^*(\omega) = 1/\varepsilon^*(\omega) = M' + \mathrm{i}M''$$
$$= M_\infty \left[1 - \int_0^\infty \left(-\frac{\mathrm{d}\Phi(t)}{\mathrm{d}t} \right) \exp(-\mathrm{i}\omega t)\mathrm{d}t \right] \tag{16}$$

where $M_\infty = (\varepsilon_\infty)^{-1}$ is the asymptotic value of $M'(\omega)$; and $\Phi(t)$ is the time evolution of electric field within the material. $\Phi(t)$ is also called Kohlrausch–Williams–Watts (KWW) function, which can be stated as

$$\Phi(t) = \exp\left(-\frac{t}{\tau} \right)^{\beta}, \quad 0 < \beta < 1 \tag{17}$$

The smaller the value of β, the greater the deviation with respect to Debye-type relaxation. Figures 11 and 12 show that the modulus peak shifts towards higher-frequency side with increasing temperature. $M'(\omega)$ shows a dispersion tending toward M_∞ (the asymptotic value of $M'(\omega)$ at higher frequencies) (Fig. 11). The nature of the variation indicates that the electrical properties of the material arise due to the bulk (intragrain). It shows a very low value (nearly zero) in the low-frequency region and a higher value in the high-frequency region due to continuous dispersion on increasing frequency. In the low-temperature region, the value of M' increases with increase in frequency and decreases with rise in temperature in slow rate. While in the high-temperature region, the value of M' increases rapidly with increase in both temperature and frequency. It may be contributed to the conduction phenomena due to short-range mobility of charge carriers. This implies the lack of a restoring force for flow of charge under the influence of a steady electric field.

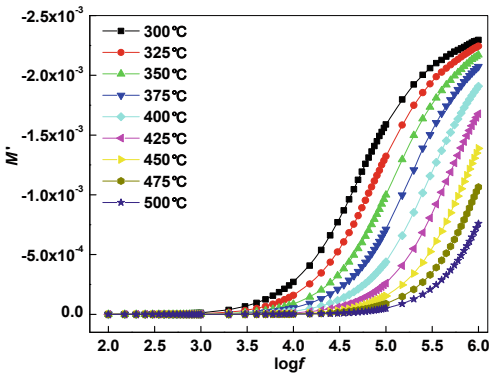

Fig. 11 Variation of real part of modulus with log f at different temperatures.

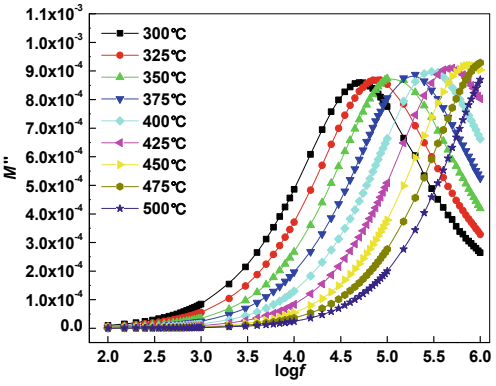

Fig. 12 Variation of imaginary part of modulus with log f at different temperatures.

Figure 13 shows the normalized imaginary part $M''/M''_{\max}$ of the complex modulus as a function of logarithmic frequency ($\log(f/f_{\max})$). It is also called the master curve as it best explains the dielectric activities going inside the material. It is found that with increase in frequency there is a sharp peak obtained at frequency of 75×10^4 Hz. In the left side of the peak, carriers are mobile in nature, and in the right side of the peak they are confined to a potential well. At the peak point, relaxation of the material is defined as

$$2\pi\tau f = 1 = RC \tag{18}$$

where R and C are the resistance and capacitance, respectively. In Li_2TiO_3, the mobile charge carriers are Li^+ ions present in the material.

$$Li^+ + TiO_2 + 1/2O_2 + 2e = Li_2TiO_3 \tag{19}$$

Figure 14 shows the variation of M'' with M' at different temperatures from 300 ℃ to 500 ℃. It shows a complete semicircle overlapping each other. The overlapping in the case of M'/M'' shows a strong evidence of long range of conductivity. It also shows that all dynamic processes occurring at different frequencies exhibit the same thermal activation energy.

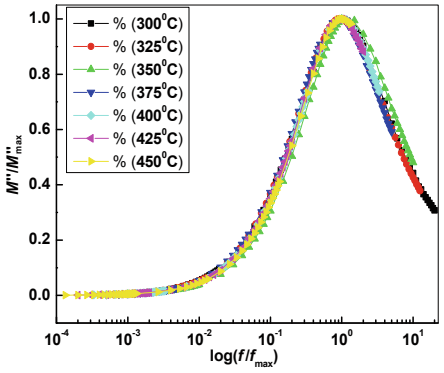

Fig. 13 Modulus master curves of Li_2TiO_3 nanoceramics at different temperatures.

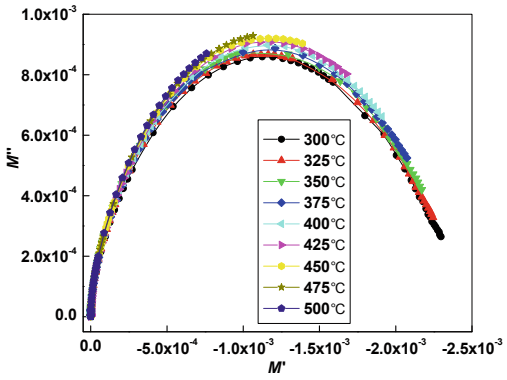

Fig. 14 Complex modulus plot of Li_2TiO_3 nanoceramics at different temperatures.

5.5 Electrical permittivity

As we know in the case of dielectric relaxation with a single relaxation time, the complex permittivity can be explained as

$$\varepsilon^*(\omega) = \varepsilon' - i\varepsilon''(\omega) = \varepsilon_\infty + \frac{\varepsilon_s - \varepsilon_\infty}{1 + i\omega\tau} \tag{20}$$

where ε_s and ε_∞ are low and high frequency values of ε', respectively; τ is the relaxation time; and ω is the relaxation frequency.

Figure 15 shows the temperature dependence of real part of dielectric permittivity $\varepsilon^*=\varepsilon'-i\varepsilon''$ for various frequencies. It is found that there is no local maximum in ε' as temperature increases. It confirms that no phase change transition occurs in the given temperature range. The real part of permittivity ε' increases sharply in lower frequency, and in high frequencies it shows almost parallel to temperature axis. Figure 16 shows the frequency dependence of real part of complex permittivity from 300 ℃ to 500 ℃. It is clear from Fig. 16 that, with increase in frequency as well as temperature, the value of ε' decreases and all the values merge at higher frequencies. Properties such as dielectric constant, dielectric loss and conductivity are closely related to the microstructure of the sample. The frequency-dependent dielectric permittivity shows the normal behavior of dielectric material having mobile charge carriers (i.e., ions and electrons). The fall in dielectric constant indicates that the polarization does not occur instantaneously with the application of electric field as charge possesses inertia. The angular frequency dependence of the dielectric constant (ε) of Li_2TiO_3 is shown in Fig. 16. The nature of the dielectric permittivity for free dipoles oscillating in an alternating field may be described in the following way. At very low frequencies ($\omega \ll 1/\tau$, τ is the relaxation time), dipoles follow the field and we have $\varepsilon'=\varepsilon_s$ (value of the dielectric constant at quasistatic fields). As the frequency increases (with $\omega<1/\tau$), dipoles begin to lag behind the field and ε_0 slightly decreases. When frequency reaches the characteristic frequency ($\omega=1/\tau$), the dielectric constant drops (relaxation process). At very high frequencies ($\omega \gg 1/\tau$), dipoles can no longer follow the field and $\varepsilon' \approx \varepsilon_\infty$ (high-frequency value of ε'). At all temperatures, dielectric constant gradually decreases with increasing frequency. The dielectric constant at low frequency is

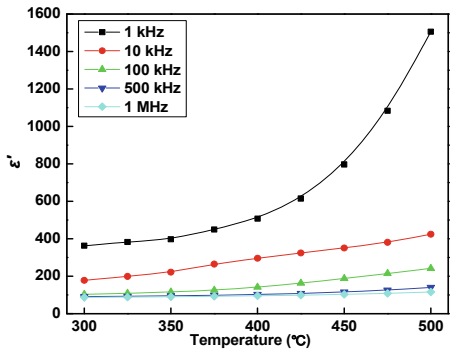

Fig. 15 Temperature dependence of real part of dielectric permittivity of Li_2TiO_3.

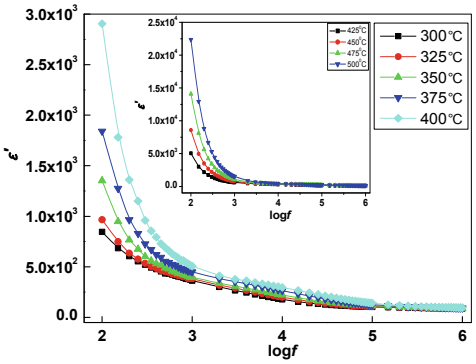

Fig. 16 Frequency dependence of real part of dielectric permittivity of Li_2TiO_3.

rather high, and is found to decrease with frequency at first and then becomes more or less stabilized. The high value of ε' at frequencies lower than 1 kHz, which increases with decreasing frequency and increasing temperature, corresponds to bulk effect of the system. This indicates the thermally activated nature of the dielectric relaxation of the system.

6 Discussions

From the XRD, we describe that the β phase of the material exists in 700 ℃ and there is no secondary phase change existing in the material. Due to this, the grain size of the material is well distributed along the entire surface. As we observe from the graphs, it requires a detailed discussion about the electrical properties of the material. The material prepared by high energy ball milling shows uniform distribution of grain size throughout the surface. CIS technique used in the study separates grain and grain boundary contributions in the material. Both the grain and grain boundary resistances decrease with increase in temperature. We have used an equivalent circuit to describe the electrical phenomena occurring in the material. It can be noticed that, as a polycrystalline material, it shows both grain and grain boundary properties at different time constants at high temperatures leading to two successive semicircles. At low temperatures, bulk effects are observed showing the higher rate of resistance in the material. The resistivity of the material decreases as temperature increases. From the complex impedance graph, there is a broadening of peaks showing that the relaxation process occurs due to the presence of immobile species at low temperatures and vacancies at higher temperatures.

It confirms that at high temperatures, conductivity of the material increases, which closely relates to the release of tritium in the material. It can also be noticed that the release of Li^+ ions from the material also depends on the bulk and grain boundary properties of the material. The grain boundary conductivity increases with temperature and shows a lower activation energy (0.86 eV). As we know, the electro negativity of lithium is low (0.98) as compared to that of titanium (1.54), showing extra electron in the conduction band. The electronic configurations of both the materials are shown as Li—[He] $2s^1$ and Ti—[Ar] $3d^24s^2$. It shows that the atomic radius and core charge of lithium are quite small as compared to those of titanium. As it has one electron in the outermost shell, the electron drives easily to the most electron negative material (Ti). The electron affinity of Ti is more as Li shows gaining of electron from the conduction band. It is well understood by grain boundary diffusion. The grain boundary (GB) is defined as the interface between two crystals (or grains). The features of GB diffusion are low migration barriers and high concentration of diffusion-mediating defects due to incomplete bonding or disorder. Thus the diffusivity value along a GB is higher than that within grains. Diffusion of a Li^+ ion into Ti particle is strongly dependent upon the interaction potential between the Li^+ ion and the host material structure. Li^+ ion transport in the material depends on the total potential energy of the diffusing ion in the crystal. First principle and ab initio study prove the ion transport mechanism in lithium titanate. As we know, the electrical conduction in a semiconductor is a thermally activated phenomenon which usually follows an Arrhenius-type relationship. The conductivity is due to the Li^+ ion

transport in the material. The electronic conductivity is expected to be more significant in the material and is concluded from the optical properties of lithium titanate and electrode polarization. Oxygen mobility in the material is not significant in the electronic conduction, as cubic close packing is essentially not a prospect for O^{2-} ion mobility. From the graph, it is clearly seen that conductivity dependences with temperature for the materials studied cannot be described by a single straight line which obeys conductivity equation:

$$\sigma = \frac{\gamma N e^2 c(1-c) z^2 a^2 \upsilon}{kT} \exp\left(\frac{\Delta s}{k}\right) \exp\left(-\frac{E_a}{kT}\right) \quad (21)$$

where γ is the correlation factor for the jumps; N is the total number of available sites per unit volume; e is the elementary charge; c is the fraction of mobile ions at these sites; z is the valence of charge carriers; a is the distance between the nearest sites; υ is the ion vibration frequency close to 10^{13} Hz; Δs is the change of entropy; k is the Boltzmann constant; and E_a is the activation energy. From the structure of lithium titanate, the lithium ion mobility can occur in parrel to the *a*–*b* plane; however, it is limited to the *c* direction by oxygen and titanium ion layers. Thus conductivity in lithium titanate can be limited if lithium metatitanate crystal takes an orientation in the *a*–*b* plane being parallel to the electrode surface [28]. The conductivity in Li^+ ion is well set in the positions of lithium in the octahedral sites. The conductivity occurs when there is a movement of ions from tetrahedral interstices to the adjacent octahedral positions. At higher temperatures, the conductivity values increase which confirms that there is a drift of large number of lithium ions from their original positions leading to ionic motion in the material. From the conductivity graph, it is noticed that there is a first order phase change in the material occuring in the temperature range between 400 ℃ and 500 ℃. There is no clear explanation regarding the disordering in conductivity reported as it can be assumed that due to heating it creates some ion movement in the material. It can be assumed that mostly two prominent types of conduction take place for the DC temperature dependence conductivity curve. At low temperatures, defects possibly occur by surface modifications, whereas at high temperatures, jumping of Li^+ ion from tetrahedral to octahedral might be the cause. From the conductivity graph, the region having lower slope is associated with extrinsic conductivity, whereas the region having higher slope gets the intrinsic conductivity. It can be thought that migration of Li^+ ions to the interstitial sites creates vacancies which in turn show conduction in the material. The possible migration of ions in (001) crystal plane in monoclinic structure has been noticed. There is also a possible chance that in the case of sample preparation, there might be some deficiency of lithium which gives to the vacancy in the material. From the figure, it is concluded that frequency plays an important role in Li^+ ion migration in the material. The variety of potential barrier surrounded by Li^+ ions enhances the conductivity. At higher frequencies, the barrier height is shorter and migration of ions occurs to the next empty sites.

7 Conclusions

The sample has monoclinic structure as confirmed from XRD technique. Detailed studies of electrical properties indicate that the material exhibits: (1) temperature-dependent relaxation phenomena; (2) conduction due to bulk and grain boundary present inside the material; (3) electrical transport governed in the material by appearance of two distinct semicircles in the complex impedance spectrum (T > 300 ℃); (4) NTCR-type behavior. The present research work shows that the formation of monoclinic single-phase Li_2TiO_3 nanoceramic prepared by high energy ball milling has lower calcination temperature (as compared to solid-state reaction). From the electrical properties, bulk conduction and grain boundary conduction processes are shown. The activation energies are calculated from DC conductivity and relaxation time, showing that charge carriers are almost the same. This suggests that the similar types of charge carriers are responsible for both the electrical conduction and electrical relaxation phenomena inside the material. The activation energy from DC conductivity plot suggests the possibility of electrical conduction due to Li^+ ions present inside the material. Modulus plot suggests the non-exponential type conductivity inside the material. It can be concluded that this material is best suitable for Li^+-ion battery as well as tritium release inside the fusion blanket. With high conductivity and low activation energy, the grain conduction gives high rate of tritium release from the material.

Acknowledgements

We thank the Board of Research in Fusion Science and Technology (BRFST), Institute for Plasma Research Gandhinagar, India for financial support of the research (Grant No. NFP/MAT/F10/01).

References

[1] Alvani C, Casadio S, Contini V, *et al*. Li_2TiO_3 pebbles reprocessing, recovery of ^6Li as Li_2CO_3. *J Nucl Mater* 2002, **307–311**: 837–841.

[2] Kopasz JP, Miller JM, Johnson CE. Tritium release from lithium titanate, a low-activation tritium breeding material. *J Nucl Mater* 1994, **212–215**: 927–931.

[3] Roux N, Avon J, Floreancing A, *et al*. Low-temperature tritium releasing ceramics as potential materials for the ITER breeding blanket. *J Nucl Mater* 1996, **233–237**:1431–1435.

[4] Dienst W, Zimmermann H. Investigation of the mechanical properties of ceramic breeder materials. *J Nucl Mater* 1988, **155–157**: 476–479.

[5] Rasneur B, Charpin J. Chemical properties of lithium ceramics: Reactivity with water and water vapour. *J Nucl Mater* 1988, **155–157**: 461–465.

[6] Hofmann P, Dienst W. Compatibility studies of metallic materials with lithium-based oxides. *J Nucl Mater* 1988, **155–157**: 485–490.

[7] Noda K, Ishii Y, Matsui H, *et al*. A study of tritium behavior in lithium oxide by ion conductivity measurements. *Fusion Eng Des* 1989, **8**: 329–333.

[8] Roux N, Tanaka S, Johnson C, *et al*. Ceramic breeder material development. *Fusion Eng Des* 1998, **41**: 31–38.

[9] Gierszewski P. Review of properties of lithium metatitanate. *Fusion Eng Des* 1998, **39–40**: 739–743.

[10] Hegeman JBJ, van Essen EDL, Jong M, *et al*. Thermomechanical behaviour of ceramic breeder pebble stacks for HICU. *Fusion Eng Des* 2003, **69**: 425–429.

[11] Tsuchiya K, Kawamura H, Takayama T, *et al*. Control of particle size and density of Li_2TiO_3 pebbles fabricated by indirect wet processes. *J Nucl Mater* 2005, **345**: 239–244.

[12] Fehr Th, Schmidbauer E. Electrical conductivity of Li_2TiO_3 ceramics. *Solid State Ionics* 2007, **178**: 35–41.

[13] Kinjyo T, Nishikawa M, Enoeda M, *et al*. Tritium diffusivity in crystal grain of Li_2TiO_3 and tritium release behavior under several purge gas conditions. *Fusion Eng Des* 2008, **83**: 580–587.

[14] Wu X, Wen Z, Xu X, *et al*. Fabrication and improvement of the density of Li_2TiO_3 pebbles by the optimization of a sol–gel method. *J Nucl Mater* 2009, **393**: 186–191.

[15] Sinha A, Nair SR, Sinha PK. Single step synthesis of Li_2TiO_3 powder. *J Nucl Mater* 2010 **399**: 162–166.

[16] Vittal Rao TV, Bamankar YR, Mukerjee SK, *et al*. Preparation and characterization of Li_2TiO_3 pebbles by internal gelation sol–gel process. *J Nucl Mater* 2012, **426**: 102–108.

[17] Ohno H, Konishi S, Nagasaki T, *et al*. Correlation behavior of lithium and tritium in some solid breeder materials. *J Nucl Mater* 1985, **133–134**: 181–185.

[18] Deptuła A, Łada W, Olczak T, *et al*. Preparation of lithium titanate by sol–gel method. *Nukleonika* 2001, **46**: 95–100.

[19] Tsuchiya K, Kawamura H, Fuchinoue K, *et al*. Fabrication development and preliminary characterization of Li_2TiO_3 pebbles by wet process. *J Nucl Mater* 1998, **258–263**: 1985–1990.

[20] Jung C-H. Sintering characterization of Li_2TiO_3 ceramic breeder powders prepared by the solution combustion synthesis process. *J Nucl Mater* 2005, **341**: 148–152.

[21] Lulewicz JD, Roux N. Fabrication of Li_2TiO_3 pebbles by the extrusion–spheronisation–sintering process. *J Nucl Mater* 2002, **307–311**: 803–806.

[22] Mandal D, Sathiyamoorthy D, Vinjamur M. Experimental measurement of effective thermal conductivity of packed lithium-titanate pebble bed. *Fusion Eng Des* 2012, **87**: 67–76.

[23] Sinclair DC, West AR. Impedance and modulus spectroscopy of semiconducting $BaTiO_3$ showing positive temperature coefficient of resistance. *J Appl Phys* 1989, **66**: 3850.

[24] Lanfredi S, Rodrigues ACM. Impedance spectroscopy study of the electrical conductivity and dielectric constant of polycrystalline $LiNbO_3$. *J Appl Phys* 1999, **86**: 2215.

[25] Barsoukov E, Macdonald JR. *Impedance Spectroscopy*: *Theory*, *Experiment*, *and Applications*, 2nd, edn. New York: John Wiley & Sons, 2005.

[26] Wang CC, Wang C, Zeng R, *et al*. Intergrain connectivity of MgB_2 ceramics studied by impedance analysis. *J Appl Phys* 2010, **108**: 023901.

[27] Argall F, Jonscher AK. Dielectric properties of thin films of aluminium oxide and silicon oxide. *Thin Solid Films* 1968, **2**: 185–210.

[28] Vītiņš Ģ, Ķizāne G, Lūsis A, *et al*. Electrical conductivity studies in the system Li_2TiO_3–$Li_{1.33}Ti_{1.67}O_4$. *J Solid State Electr* 2002, **6**: 311–319.